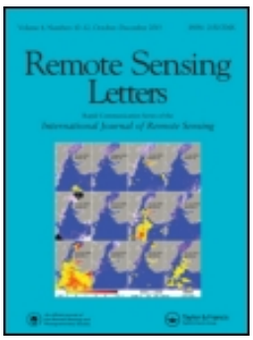

Remote Sensing Letters

ISSN: 2150-704X (Print) 2150-7058 (Online) Journal homepage: http://www.tandfonline.com/loi/trsl20

Development of a multi-scale object-based shadow detection method for high spatial resolution image

Hui Luo, Le Wang, Zhenfeng Shao & Deren Li

To cite this article: Hui Luo, Le Wang, Zhenfeng Shao & Deren Li (2015) Development of a multi-scale object-based shadow detection method for high spatial resolution image, Remote Sensing Letters, 6:1, 59-68, DOI: 10.1080/2150704X.2014.1001079

To link to this article: https://doi.org/10.1080/2150704X.2014.1001079

Published online: 19 Jan 2015.

Remote Sensing Letters, 2015
Vol. 6, No. 1, 59–68, http://dx.doi.org/10.1080/2150704X.2014.1001079

Taylor & Francis
Taylor & Francis Group

Development of a multi-scale object-based shadow detection method for high spatial resolution image

Hui Luo[a], Le Wang[a,b,c]*, Zhenfeng Shao[a,c], and Deren Li[a,c]

[a]*State Key Laboratory of Information Engineering in Surveying, Mapping and Remote Sensing (LIESMARS), Wuhan University, Wuhan, China;* [b]*Department of Geography, The State University of New York at Buffalo, Buffalo, NY, USA;* [c]*Collaborative Innovation Center of Geospatial Technology, Wuhan University, Wuhan, China*

(*Received 24 September 2014; accepted 16 December 2014*)

Effective treatment of shadows generated by the obstruction of trees and buildings is an inevitable task for extracting detailed spectral and spatial information from urban high-resolution images. Object-based shadow detection methods can take full advantages of spatial features in the urban very high resolution (VHR) images. However, the effect of different segmentation parameters for detecting shadows has not been well studied. In this study, we proposed an object-based method for shadow detection on urban high-resolution image and addressed quantitative assessment of segmentation. In proposed object-based method, a multi-scale segmentation method, known as fractal net evolution approach (FNEA), was employed to generate primitive objects; then, three spectral properties of shadows were fused based on Dempster–Shafer (D–S) evidence theory to identify shadows. In quantitative assessment, a method for ordering significance of parameters and deriving optimal parameters based on orthogonal experimental design was proposed to evaluate the impact of different segmentation variables on the accuracy of shadow detection. Experimental results indicate that the best overall accuracy (OA) for shadow detection of our method was 89.60% after segmentation parameters' optimization and scale is the most influential parameter of FNEA segmentation parameters in determining the performance of shadow detection.

1. Introduction

With the development of remote-sensing technique, very high resolution (VHR) images have been playing an increasing role in the field of earth observation (Zhou and Troy 2008). However, shadows generated by the obstruction of trees and buildings are inevitable in the urban VHR images, which not only bring challenges to the following image processing, but also could provide geometric and semantic information of objects (Arévalo, González, and Ambrosio 2008). Therefore, developing a method for shadow detection from the urban VHR images have attracted increasing attention.

Property-based shadow detection methods (Arévalo, González, and Ambrosio 2008; Tsai 2006; Chung, Lin, and Huang 2009) with invariable colour model have been intensively studied in the past, since they can be directly applied to the original remote-sensing image data without any a priori information (Adeline et al. 2013). Generally, they can be categorized into two types: pixel-based methods (Tsai 2006; Huang, Xie, and Tang 2004) and object-based methods (Arévalo, González, and Ambrosio 2008; Zhu, Xu, and Han 2007).

Most pixel-based methods derive shadow information with the use of primarily spectral and radiometric features (Adeline et al. 2013). Although the pixel-based methods

*Corresponding author. Email: lewang@buffalo.edu

are simple to calculate and have high efficiency, they suffer from the problems of incomplete candidate shadow areas and 'salt and pepper' noise. In contrast, object-based shadow detection methods have been found to be more effective in handling high-resolution imagery than their pixel-based counterparts owing to the fact that spatial information can be more readily incorporated, and thus homogenous candidate shadow areas can be made available by using segmentation steps (Benz et al. 2004).

Segmentation is a crucial step in object-based method (Feitosa et al. 2006), since different segmentation parameter settings will directly affect the final classification or target detection accuracy. Thus, it is important to evaluate the impact of different segmentation parameters on the final accuracy. The multi-scale segmentation algorithm, namely fractal net evolution approach-FNEA (Baatz and Schäpe 2000), is one of the most popular segmentation algorithms (Feitosa et al. 2006; Liu and Xia 2010; Wang, Sousa, and Gong 2004). Although FNEA has been successfully applied in ecosystem features (Karl and Maurer 2010; Addink, Jong, and Pebesma 2007) and land-cover/land-use mapping (Benz et al. 2004), few studies about object-based shadow detection with shadows' invariable colour features incorporated with the FNEA have been reported. In addition, given the fact that FNEA includes a number of parameters, it is worthwhile to investigate how these parameters affect on the final shadow detection results. To this end, our overall objectives are two fold: (1) to develop a new object-based method for shadow detection with FNEA segmentation; (2) to assess the impact of various FNEA segmentation parameters on the accuracy of shadow detection. In this paper, we propose an object-based shadow detection with Dempster–Shafer (D–S) evidence theory (Shafer 1992) method (OBSDD-S method) to combine different shadows' spectral properties. Then an approach for parameters' influence evaluation based on orthogonal experimental design is proposed to acquire the order of the FNEA segmentation parameter by their significance, and obtain optimal parameters for OBSDD-S method.

2. Object-based shadow detection with the high-resolution image

2.1. *Procedure of object-based shadow detection with the high-resolution image*

There are two steps in the OBSDD-S method. First, a multi-scale segmentation method is employed to segment the image so as to derive the primitive image objects. Second, these objects are further classified as shadows or non-shadows based on a criterion, which is obtained by D–S evidence theory in fusion of three spectral properties of shadows. In this paper, an accuracy assessment for shadow detection according to Tsai (2006) was adopted, including overall accuracy (OA), commission/omission error, and Kappa coefficient.

The flowchart of our proposed method is illustrated in Figure 1. The procedures of this method are shown below:

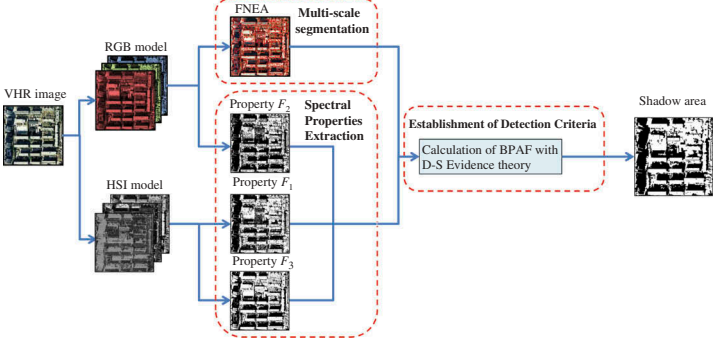

Figure 1. Flowchart of proposed object-based shadow detection method with the VHR remote-sensing image.

(1) Multi-scale segmentation using high-resolution image with RGB (Red Green Blue) colour model, described in Section 2.2;
(2) Extraction of candidate shadow areas according to three spectral properties F_1, F_2, and F_3, which will be defined in Section 2.3;
(3) Detection of shadows based on establishments of the criteria that incorporates basic probability assignment functions (BPAF) in D–S evidence theory. The definition of BPAF is presented in Section 2.4.

2.2. Multi-scale segmentation

The multi-scale segmentation algorithm, namely FNEA embedded in Definiens™, is a bottom-up region-growing technique to form homogenous objects starting with single pixel (Benz et al. 2004). The final FNEA segmentation result is optimized by numerous iterative steps. In each step, a pair of adjacent objects is merged as a new image object, which yields the minimum growth of heterogeneity measurement f_m. The merging process will stop when f_m exceeds a user-defined threshold f decided by scale parameter s, which determines the average size of final objects (Liu and Xia 2010). f is assigned as the square of s (Tong et al. 2012) in this paper. f_m is obtained by calculating a weighted sum of colour and shape heterogeneity (colour/ shape weight: w_{colour}/w_{shape}, s.t. $w_{colour} + w_{shape} = 1$).Weight of each spectral band (for aerial image in this study, weight of each band is w_R, w_G, and w_B respectively, s.t. $w_R + w_G + w_B = 1$) is involved in the calculation of colour heterogeneity. Similarly, shape heterogeneity is decided with regard to the weight of smoothness and compactness ($w_{smooth}/w_{compact}$, s.t. $w_{smooth} + w_{compact} = 1$). Therefore, there are eight parameters (w_{colour}, w_{shape}, w_{smooth}, $w_{compact}$, w_R, w_G, w_B, and s) in the FNEA segmentation. All the parameters are non-negative, and all the weights are smaller than 1.

2.3. Selections of spectral properties in shadow detection

Spectral properties of shadows are effective in detecting shadows (Tsai 2006). In this paper, we select three invariable shadows' properties calculated from RGB and HSI (Hue Saturation Intensity) colour model (Tsai 2006; Zhu, Xu, and Han 2007).

(1) F_1: Hue in HSI colour model (Gonzales and Woods 2006). The definition of hue is shown as Equation (1). *R, G,* and *B* denotes the red, green, and blue band values in RGB colour model, respectively. Generally, the difference of the hue values between shadows and non-shadows is significant.

$$F_1 = \begin{cases} \theta & G \geq B \\ 2\pi - \theta & G < B \end{cases}, \theta = \cos^{-1}\left\{ \frac{1}{2}[(R-G)+(R-B)] \Big/ [(R-G)^2+(R-B)(G-B)]^{\frac{1}{2}} \right\} \tag{1}$$

(2) F_2: F_2 equals the difference between blue and green bands. It is a measurement to describe the degree of colour inclined to blue band.
(3) F_3: Difference between intensity and saturation in HSI model. I represents intensity and S denotes saturation, as Equation (2).

$$\begin{cases} F_3 = I - S \\ S = 1 - 3 \times [\min(R, G, B)]/(R + G + B) \\ I = (R + G + B)/3 \end{cases} \tag{2}$$

K-means classification is selected to classify the image of three shadows' properties into two classes: shadows and non-shadows, respectively. For each property F_i (i = 1, 2, 3) image after classification, there is a binary image (candidate shadow and non-shadow

areas are assigned as 0 and 1 in the binary image, respectively). These binary images are the input data of forming the criteria in shadow detection based on D–S evidence theory, which is described in Section 2.4.

2.4. Object-based shadow detection with Dempster–Shafer evidence theory

Because of the complexity of real land cover, it is hard to extract shadows with only one single spectral property or simple intersection of the three spectral properties. In order to increase the accuracy of shadow detection, it is feasible to set a criterion taking account of complementarities of the three spectral properties. To this end, D–S evidence theory (Lu, Trinder, and Kubik 2006; Zhu, Xu, and Han 2007) was adopted in our proposed method.

D–S evidence theory employs BPAF in fusion of the probability of each evidence to describe the probability of an event happened (Shafer 1992), e.g. fusing the probability of the object being shadow in each feature to determine the final probability in this paper. A finite set of propositions is defined as Θ, whose power set is 2^{Θ}. Supposing A is an non-empty subset of 2^{Θ}, and $m(A)$ denotes the BPAF of A, representing the degree of belief in the proposition depicted by A. BPAF m: $2^{\Theta} \rightarrow [0, 1]$, satisfying two conditions: $m(\varnothing) = 0$ and $\sum_{A \in 2^{\Theta}} m(A) = 1$. For q pieces of independent evidences and g types of A_r ($\forall A_r \in 2^{\Theta}$, $A_r \neq \varnothing$, and $r = 1, 2\ldots, g$), $m_n(B_n)$ denotes BPAF calculated from the evidence n ($1 \leq n \leq q$, $q \geq 3$), and $\exists B_n \in \{A_1, A_2, \ldots, A_g\}$. Thus, $m(A)$ is defined as Equation (3), denoting the A's probability in fusion of q pieces of evidences' probability.

$$m(A) = \left[\sum_{B_1 \cap B_2 \ldots \cap B_q = A} \left(\prod_{1 \leq n \leq q} m_n(B_n) \right) \right] \Bigg/ \left[1 - \sum_{B_1 \cap B_2 \ldots \cap B_q = \varnothing} \left(\prod_{1 \leq n \leq q} m_n(B_n) \right) \right] \tag{3}$$

In this study, there are three evidences (F_1, F_2, and F_3). Supposing $\Theta = \{h_0, h_1\}$, where h_0 represents the objects of shadow areas and h_1 addresses that of non-shadow areas. So, $\{h_0\}$, $\{h_1\}$, and $\{h_0, h_1\}$ are three non-empty subset of 2^{Θ}. There is a series of objects of the image O_j ($j = 1,2,\ldots,k$) after multi-segmentation. $m_i^j(h_0)$, $m_i^j(h_1)$, and $m_i^j(h_0, h_1)$ are defined as Equation (4) (Zhu, Xu, and Han 2007).

$$\begin{cases} m_i^j(h_0) = \left(N^j_{\text{ShawdowCount},\, i} \Big/ N^j_{\text{TotalCount},\, i} \right) p_i \\ m_i^j(h_1) = \left(1 - N^j_{\text{ShawdowCount},\, i} \Big/ N^j_{\text{TotalCount},\, i} \right) p_i \\ m_i^j(h_0, h_1) = 1 - p_i \end{cases} \tag{4}$$

where p_i is the confidence of property F_i ($i = 1, 2, 3$). In this letter, p_i is assigned as OA of the corresponding binary image in property F_i. $N^j_{\text{ShawdowCount},\, i}$ and $N^j_{\text{TotalCount},\, i}$ denotes the candidate shadow pixel numbers and total pixel numbers in object j for property F_i, respectively. The $m^j(h_0)$, $m^j(h_1)$, and $m^j(h_0, h_1)$ combined with three properties can be calculated by Equations (3) and (4). If the Equation (5) is satisfied, the object j is detected as the shadow area (Zhu, Xu, and Han 2007).

$$\begin{cases} m^j(h_0) > m^j(h_1) \\ m^j(h_0) > m^j(h_0, h_1) \end{cases} \tag{5}$$

2.5. Evaluation of FNEA parameters' influence upon the OBSDD-S

Configurations of proper parameters for FNEA play a critical role in OBSDD-S method, but there is little research about assessing influence of various parameters in FNEA on shadow detection. So, two parts for the evaluation of influence are conducted in our paper. In the first part, the optimal five-parameter combination of FNEA segmentation (w_{colour}, w_{shape}, w_{compact},

w_{smooth}, and *f)* for the OBSDD-S method was acquired through orthogonal experimental design (OED) (Taguchi 1986; Franek and Jiang 2013). In addition, order of significance for three independent parameters (w_{colour}, $w_{compact}$, and *f*) among the five parameters were calculated by a manner derived based on OED. In the second part, the impacts of the three band weights (w_R, w_G, and w_B) in FNEA segmentation on OBSDD-S method's accuracy are tested. At the end, the optimal set of parameters for FNEA segmentation was accomplished.

(1) Part 1: Contrary to full factorial analysis, OED applies an orthogonal array to exhaustively study the independent parameters by running a limited number of experiments, which has been widely utilized in quality control and manufacturing process optimization (Taguchi 1986; Zhu et al. 2013). Generally, there are two steps in parameter learning with OED (Franek and Jiang 2013).

First, an appropriate orthogonal array is selected according to parameters setting and experiments scheme. Orthogonal array generally represents a matrix $\mathbf{L}_t(l^u)$, where t is the number of experimental runs, l is the number of sampling levels per parameter, and u is the maximum independent number of parameters involved in this matrix. Three independent parameters ($w_{compact}$, w_{colour}, and *f*) are involved in the calculation of the orthogonal array $\mathbf{L}_{25}(5^6)$ (Chen et al. 2007), because w_{smooth}, w_{shape} can be correspondingly calculated from $w_{compact}$ and w_{colour}. Only part of $\mathbf{L}_{25}(5^6)$ (Chen et al. 2007) was adopted, as shown in Table 2, because the number of independent parameters is less than the maximum independent number of parameters involved in $\mathbf{L}_{25}(5^6)$. In addition, due to the fact that w_R, w_G, and w_B have to sum to one and thus are not independent, for simplify, we set all the three weights equal to 1/3 and be invariant in this part.

Second, analysis of means (ANOM) is conducted upon 25 experimental runs to evaluate the parameters' influence, including the optimum parameters combination and order of significance among all the parameters. Specifically, average effect $\bar{E}_x$ denotes the mean of the OBSDD-S method results' OA, and OA of these results are acquired when parameter x is at level E value (five sampling levels: E = I, II, III, IV, V). If $\bar{E}_x$ is the maximum among all the average effects for x, this value at level E is considered as the optimum parameter for x. Furthermore, the significance for parameter x is decided by the difference between the maximum and minimum average effects among all levels. The bigger difference (Δ_x) means the higher significance. Beside the two steps above, if the optimum parameter combination acquired by ANOM is not one of the original parameter combinations in the orthogonal array, a confirmation test (Franek and Jiang 2013) is needed. Specifically, if the OA resulted in optimum parameters is higher than the maximum OA among the 25 runs in Table 2, these optimum parameters are accepted. If not, the parameters yielding maximum OA is considered as the final optimum parameter combination.

(2) Part 2: w_{colour}, w_{shape}, $w_{compact}$, w_{smooth}, and f were fixed as the optimal five-parameter combination obtained from the first part. Evaluation of w_R, w_G, and w_B is accomplished through adding incremental of 0.2 to each band weight, shown in the lower graph in Figure 3. The parameters, which yield maximum OA in this part, is considered as the optimum parameters.

3. Experimental results and discussion

In order to evaluate our proposed method, A WILD 15/4 UAGA-F camera aerial image from Beijing was adopted as the test image in Figure 2(*a*). This image had a size of 512 pixels × 512 pixels, and the centre of it is located at 39°52′33.98″ N, 116°27′46.99″ E. There are several land cover types in this image, such as buildings, vegetation, bare soil, and shadows.

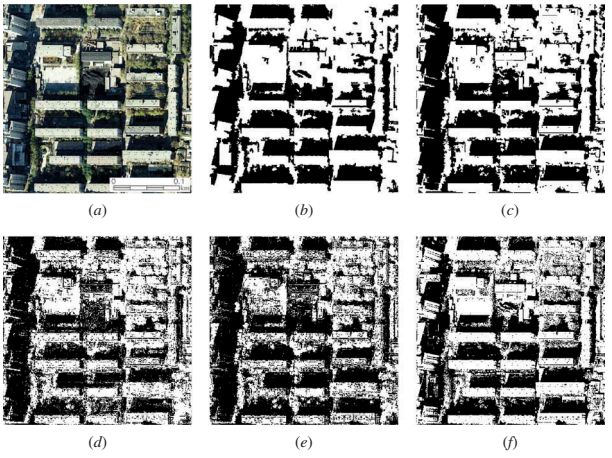

Figure 2. (*a*) The test aerial image, (*b*) reference image of shadows, (*c*) the result of the OBSDD-S method having the best performance among all the experiments, (*d*)–(*f*) candidate shadows obtained from three spectral properties of shadows (F_1, F_2, and F_3), respectively.

3.1. *Shadow detection results of the OBSDD-S*

The reference shadow result was acquired by a careful visual interpretation, shown in Figure 2(*b*). The shadow detection results of OBSDD-S is shown in Figure 2(*c*) acquired with $w_{\text{colour}} = 0.3$, $w_{\text{shape}} = 0.7$, $w_{\text{compact}} = 0.9$, $w_{\text{smooth}} = 0.1$, $f = 100$, $w_{\text{R}} = 0.2$, $w_{\text{G}} = 0.6$, and $w_{\text{B}} = 0.2$. This FNEA parameters' setting was optimized, yielding the highest OA in shadow detection (89.60%) among all the following experiments. How to obtain the optimum FNEA parameters for the OBSDD-S is illustrated in Section 3.2. We obtained candidate shadow areas for F_1, F_2, and F_3 (Figure 2(*d*)–(*f*)) after k-means classification. For Figure 2(*b*)–(*f*), the black/white areas are shadow/non-shadows areas. There are many 'speckles' in the images (Figure 2(*d*)–(*f*)), because the three candidate shadow images are extracted in a per-pixel manner through the corresponding spectral properties. The OA of these three binary images of candidate shadow (Figure 2(*d*)–(*f*)) are 78.92%, 77.67%, and 88.07% respectively, which are all lower than that of results by the OBSDD-S (Figure 2 (*c*)). It shows that our proposed method can take into consideration of the information based on three aspects of candidate shadows and obtain a better final result. For comparative purpose, two shadow detection methods from Chung, Lin, and Huang (2009) and Huang and Zhang (2012) were used in our paper. The OA of two comparative methods and our method (Figure 2(*c*)) are shown in Table 1, suggesting OBSDD-S has better performance than two comparative methods. For Chung et al.'s method, we used the parameters value recommended in their paper. Chung et al.'s method didn't have relatively high performance, which may be because of a lack of parameters optimization step in their method. Besides, Huang and Zhang's method takes advantage of the high local contrast between shadows and their neighbouring non-shadow to extract shadows. But some shadows may be misclassified as non-shadows since local contrast within the shaded areas are still existed.

Table 1. Accuracies of three methods in shadow detection for test image (Figure 2(*a*)).

Method	Chung et al.'s	Huang and Zhang's	OBSDD-S
OA(%)	68.54	85.54	89.60

3.2. Evaluation of FNEA parameters' influence upon the OBSDD-S

In this part, we use the evaluation method described in Section 2.5 to make an assessment of the influence of FNEA parameters. It should be noted that in order to evaluate the impact of various parameters on the OBSDD-S performance objectively, in the following two parts of the experiments, three parameters in D–S evidence theory (p_1 = 0.79, p_2 = 0.78, and p_3 = 0.88) were fixed, so was the input data (except segmented image after FNEA).

3.2.1. Part 1: evaluation of w_{colour}, w_{shape}, $w_{compact}$, w_{smooth}, and f

There are 25 runs, three independent parameters, and five levels for each parameter in the orthogonal array, which is as shown Table 2. In this table, OA, commission/omission error and kappa coefficient are also shown to illustrate the performance of shadow detection. w_R, w_G, and w_B are all set as 1/3 in this part of experiment, which is described in Section 2.5. The five levels for $w_{compact}$ and w_{colour} are assigned as 0.1–0.9 in the steps of 0.2, and s is sampled as 10–50 in the steps of 10. Thus, the five levels of f are 100, 400, 900, 1600, 2500, respectively. The average effects at different levels for each parameter are presented as $\overline{\mathrm{I}}_x$ to $\overline{\mathrm{V}}_x$($x = w_{compact}$, w_{colour}, and f) in Table 2. Similarly, Δ_x($x = w_{compact}$, w_{colour}, and f) are also present in Table 2 to measure the significance of its corresponding parameter.

Table 2. $w_{compact}$, w_{colour}, and f optimization based on orthogonal array (OA: overall accuracy).

Experimental run	$w_{compact}$	w_{colour}	f	OA (%)	Commission error (%)	Omission error (%)	Kappa coefficient
1	0.1	0.1	100	89.33	17.06	5.62	0.79
2	0.1	0.3	400	88.91	17.36	6.36	0.78
3	0.1	0.5	900	88.45	17.69	7.16	0.77
4	0.1	0.7	1600	88.24	18.43	6.46	0.76
5	0.1	0.9	2500	88.15	18.73	6.21	0.76
6	0.3	0.1	400	88.46	18.11	6.37	0.77
7	0.3	0.3	900	88.54	18.06	6.23	0.77
8	0.3	0.5	1600	88.65	17.78	6.38	0.77
9	0.3	0.7	2500	87.80	18.88	6.99	0.76
10	0.3	0.9	100	89.23	16.83	6.32	0.78
11	0.5	0.1	900	87.48	17.83	9.81	0.75
12	0.5	0.3	1600	87.84	19.01	6.60	0.76
13	0.5	0.5	2500	87.33	18.53	9.06	0.74
14	0.5	0.7	100	89.12	17.08	6.23	0.78
15	0.5	0.9	400	89.24	16.71	6.47	0.78
16	0.7	0.1	1600	87.78	17.64	9.25	0.75
17	0.7	0.3	2500	87.51	17.92	9.55	0.75
18	0.7	0.5	100	89.40	16.52	6.34	0.79
19	0.7	0.7	400	89.48	16.33	6.43	0.79
20	0.7	0.9	900	88.76	17.63	6.32	0.77
21	0.9	0.1	2500	85.44	19.15	13.72	0.70
22	0.9	0.3	100	89.58	16.35	6.10	0.79
23	0.9	0.5	400	89.56	16.23	6.36	0.79
24	0.9	0.7	900	89.15	17.08	6.13	0.78
25	0.9	0.9	1600	88.62	17.94	6.21	0.77
$\overline{\mathrm{I}}_x$	88.61	87.70	89.33				
$\overline{\mathrm{II}}_x$	88.54	88.48	89.13				
$\overline{\mathrm{III}}_x$	88.20	88.68	88.48				
$\overline{\mathrm{IV}}_x$	88.59	88.76	88.23				
$\overline{\mathrm{V}}_x$	88.47	88.80	87.25				
Δ_x	0.41	1.10	2.08				
The order of significance	$f > w_{colour} > w_{compact}$						
Optimal level before confirmation test	$w^{\mathrm{I}}_{compact}$, w^{V}_{colour}, f^{I}			Final optimal level		$w^{\mathrm{V}}_{compact}$, w^{II}_{colour}, f^{I}	

From Table 2, we can make two conclusions based on ANOM described in Section 2.5:

(1) The significance of a parameter is decided by its range of average effect at each level, as shown in Table 2. So, our study reveals that the order of parameters' significance is $f > w_{colour} > w_{compact}$. It illustrates that scale parameter is a very important parameter in FNEA for shadow detection, which can be also found in Benz et al. (2004).

(2) The optimal level for parameter x is determined by the maximum value of $\bar{I}_x$ to $\overline{V}_x$ (highlighted by dash box in Table 2). To this end, Table 2 indicates that the optimal value for $w_{compact}$, w_{colour}, and f are 0.1, 0.9, and 100, respectively. Since this optimal parameter set is not same as any parameter combination among the 25 runs, a confirmation test is needed. The OA of confirmation test ($w_{compact} = 0.1$, $w_{colour} = 0.9$, $f = 100$, and $w_R = w_G = w_B = 1/3$) is 89.27%, which is lower than the maximum OA (the 22nd run's OA: 89.58%, highlighted by dash box in Table 2) among the 25 runs. Thus, the 22nd parameter combination ($w_{compact} = 0.9$, $w_{colour} = 0.3$, and $f = 100$) is selected as the final optimal parameters for this part of experiments. According to Table 2, the commission/omission error of the 22nd run is the third/second lowest among all the 25 runs. It shows a good balance between the over-detection and under-detection for shadow.

3.2.2. *Part 2: evaluation of w_R, w_G, w_B*

In this part of experiments, w_{colour}, w_{shape}, $w_{compact}$, w_{smooth}, and f were assigned to 0.3, 0.7, 0.9, 0.1, and 100, which are the optimal five-parameter combination obtained from the first part experiment. Analysis of w_R, w_G, and w_B was conducted according to method in Section 2.5. Hereby, the scheme of value assignment for w_R, w_G, and w_B (the lower figure), and results of OA for the OBSDD-S method acquired with its corresponding combination of w_R, w_G, and w_B (the top figure) is shown in Figure 3. Specifically, for the lower figure, the height of bar in

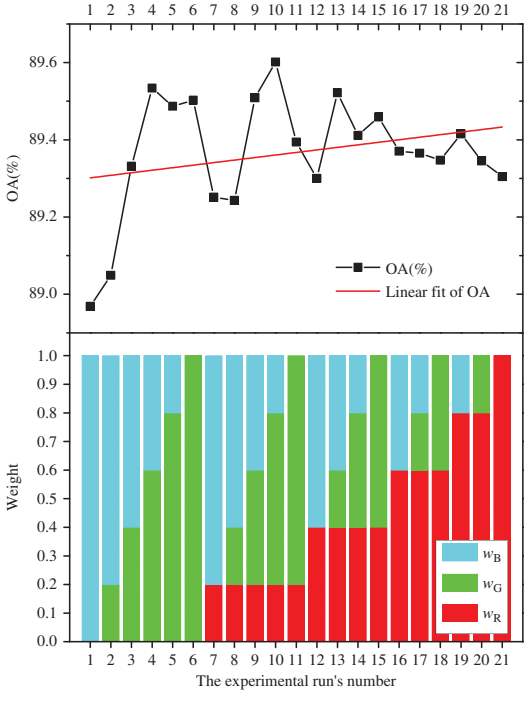

Figure 3. The scheme of value assignment for w_R, w_G, and w_B (the lower figure), and results of OA for OBSDD-S method acquired with its corresponding combination of w_R, w_G, and w_B (the top figure).

each colour denotes the weight value of its corresponding band (e.g. w_R, w_G, and w_B is 0.2, 0.2, and 0.6 in the 8th experiment, respectively). The red line in the top figure is the linear fit of OA ($y = 0.00658x + 89.29484$) for 21 runs in this part. It indicates that there is an ascending trend of OA when w_R increases. The parameter combination of 10th experiment ($w_{colour} = 0.3$, $w_{shape} = 0.7$, $w_{compact} = 0.9$, $w_{smooth} = 0.1$, $f = 100$, $w_R = 0.2$, $w_G = 0.6$, and $w_B = 0.2$) was considered as the final optimal parameters for OBSDD-S method. Because the 10th experiment not only has the highest OA value (89.60%) among all the 21 tests, but also has a better performance than the maximum OA (89.58%) in the part 1 experiment.

Experimental results (Table 2 and Figure 3) suggest that OBSDD-S method has good and stable performance in urban shadow detection with the VHR remote-sensing image. Besides, There is nearly no 'salt and pepper' phenomena in the results of OBSDD-S, and detected shadows are all in complete shape. Water may be misclassified as shadow by OBSDD-S method because water has the similar spectral responses with shadow (Li, Gong, and Sasagawa 2005). So removing water prior to shadow detection is necessary for water-existence study site. Furthermore, results indicate that OED is an effective method to optimize segmentation parameters in a reasonable number of experiments runs. OED could be applied in optimization of other multi-parameters approach for remote-sensing image from two aspects in the future: (1) optimal parameters calculation, which yields the best performance; (2) analysis of significance for each parameter, which derives some empirical knowledge for the following study. But a limitation of OED is that all the parameters involved in the orthogonal array should be independent. So, only Section 3.2.1 uses OED since w_R, w_G, and w_B are related to each other. We didn't iterate between part 1 and part 2 because the optimal parameter combination generated after these two parts yielding a pretty good performance (OA: 89.60%). The study about iteration optimization is our future task.

4. Conclusions

In this paper, we proposed an object-based shadows detection method with FNEA segmentation and D–S evidence theory. Results suggest that our proposed OBSDD-S method can get a good and stable performance for urban shadow detection. Until now, few literature studies OED as a parameters optimization approach for object-based processing in the VHR image. Therefore, our work focuses on the employment of OED to evaluate the impact of parameters variability in FNEA upon shadow detection and obtain the optimal combination with a limited computational cost. The results show that OED can find out the optimal parameter combination, resulting in the maximum accuracy. Furthermore, the order of parameter's significance can be obtained from OED. Scale is the most influential parameter of FNEA segmentation parameters in determining the accuracy of OBSDD-S according to the OED experiments.

Disclosure statement

No potential conflict of interest was reported by the authors.

Funding

The work was supported by the Fundamental Research Funds for the Central Universities [grant number 2012619020204]; the National Natural Science Foundation of China [grant number 61172174]; an open research grant from State Key Laboratory of Information Engineering in Surveying, Mapping and Remote Sensing (LIESMARS), Wuhan University.

References

Addink, E. A., S. M. D. Jong, and E. J. Pebesma. 2007. "The Importance of Scale in Object-Based Mapping of Vegetation Parameters with Hyperspectral Imagery." *Photogrammetric Engineering & Remote Sensing* 73 (8): 905–912. doi:10.14358/PERS.73.8.905.

Adeline, K. R. M., M. Chen, X. Briottet, S. K. Pang, and N. Paparoditis. 2013. "Shadow Detection in Very High Spatial Resolution Aerial Images: A Comparative Study." *ISPRS Journal of Photogrammetry and Remote Sensing* 80: 21–38. doi:10.1016/j.isprsjprs.2013.02.003.

Arévalo, V., J. González, and G. Ambrosio. 2008. "Shadow Detection in Colour High-resolution Satellite Images." *International Journal of Remote Sensing* 29 (7): 1945–1963. doi:10.1080/01431160701395302.

Baatz, M., and A. Schäpe. 2000. "Multiresolution Segmentation—An Optimization Approach for High Quality Multi-Scale Image Segmentation." In *Angewandte Geographische Informationsverarbeitung XII, Beiträge zum AGIT-Symposium Salzburg 2000*, 12–23. Karlsruhe: Herbert Wichmann Verlag.

Benz, U. C., P. Hofmann, G. Willhauck, I. Lingenfelder, and M. Heynen. 2004. "Multi-resolution, Object-oriented Fuzzy Analysis of Remote Sensing Data for GIS-ready Information." *ISPRS Journal of Photogrammetry and Remote Sensing* 58 (3–4): 239–258. doi:10.1016/j.isprsjprs.2003.10.002.

Chen, Y., J. Zhang, C. Yang, and B. Niu. 2007. "The Workspace Mapping with Deficient-DOF Space for the PUMA 560 Robot and its Exoskeleton Arm by Using Orthogonal Experiment Design Method." *Robotics and Computer-Integrated Manufacturing* 23 (4): 478–487. doi:10.1016/j.rcim.2006.05.007.

Chung, K., Y. Lin, and Y. Huang. 2009. "Efficient Shadow Detection of Color Aerial Images Based on Successive Thresholding Scheme." *IEEE Transactions Ongeoscience and Remote Sensing* 47 (2): 671–682. doi:10.1109/TGRS.2008.2004629.

Feitosa, R. Q., G. A. O. P. Costa, T. B. Cazes, and B. Feijo. 2006. "A Genetic Approach for the Automatic Adaptation of Segmentation Parameters." Paper presented at the Proceedings of the First International Conference on Object-Based Image Analysis, Salzburg, July 4–5.

Franek, L., and X. Jiang. 2013. "Orthogonal Design of Experiments for Parameter Learning in Image Segmentation." *Signal Processing* 93 (6): 1694–1704. doi:10.1016/j.sigpro.2012.08.016.

Gonzales, R. C., and R. E. Woods. 2006. *Digital Image Processsing*. Beijing: Publishing House of Electronics industry.

Huang, J., W. Xie, and L. Tang. 2004. "Detection of and Compensation for Shadows in Colored Urban Aerial Images." Paper presented at the 5th World Congress on Intelligent Control and Automation, Hangzhou, June 15–19, 3098–3100.

Huang, X., and L. Zhang. 2012. "Morphological Building/Shadow Index for Building Extraction from High-Resolution Imagery over Urban Areas." *IEEE Journal of Selected Topics in Applied Earth Observations and Remote Sensing* 5 (1): 161–172. doi:10.1109/JSTARS.2011.2168195.

Karl, J. W., and B. A. Maurer. 2010. "Spatial Dependence of Predictions from Image Segmentation: A Variogram-Based Method to Determine Appropriate Scales for Producing Land-Management Information." *Ecological Informatics* 5 (3): 194–202. doi:10.1016/j.ecoinf.2010.02.004.

Li, Y., P. Gong, and T. Sasagawa. 2005. "Integrated Shadow Removal Based on Photogrammetry and Image Analysis." *International Journal of Remote Sensing* 26 (18): 3911–3929. doi:10.1080/01431160500159347.

Liu, D., and F. Xia. 2010. "Assessing Object-Based Classification: Advantages and Limitations." *Remote Sensing Letters* 1 (4): 187–194. doi:10.1080/01431161003743173.

Lu, Y., J. C. Trinder, and K. Kubik. 2006. "Automatic Building Detection Using the Dempster–Shafer Algorithm." *Photogrammetric Engineering & Remote Sensing* 72 (4): 395–403. doi:10.14358/PERS.72.4.395.

Shafer, G. 1992. "The Dempster-Shafer Theory." In *Encyclopedia of Artificial Intelligence*, 2nd ed., edited by S. C. Shapiro, 330–331. New York: John Wiley & Sons.

Taguchi, G. 1986. *Introduction to Quality Engineering: Designing Quality into Products and Processes*. Tokyo: Asian Productivity Organization.

Tong, H., T. Maxwell, Y. Zhang, and V. Dey. 2012. "A Supervised and Fuzzy-based Approach to Determine Optimal Multi-resolution Image Segmentation Parameters." *Photogrammetric Engineering & Remote Sensing* 78 (10): 1029–1044. doi:10.14358/PERS.78.10.1029.

Tsai, V. J. D. 2006. "A Comparative Study on Shadow Compensation of Color Aerial Images in Invariant Color Models." *IEEE Transactions on Geoscience and Remote Sensing* 44 (6): 1661–1671. doi:10.1109/TGRS.2006.869980.

Wang, L., W. P. Sousa, and P. Gong. 2004. "Integration of Object-based and Pixel-Based Classification for Mapping Mangroves with IKONOS Imagery." *International Journal of Remote Sensing* 25 (24): 5655–5668. doi:10.1080/014311602331291215.

Zhou, W., and A. Troy. 2008. "An Object-Oriented Approach for Analysing and Characterizing Urban Landscape at the Parcel Level." *International Journal of Remote Sensing* 29 (11): 3119–3135. doi:10.1080/01431160701469065.

Zhu, J., D. A. S. Chew, S. Lv, and W. Wu. 2013. "Optimization Method for Building Envelope Design to Minimize Carbon Emissions of Building Operational Energy Consumption Using Orthogonal Experimental Design (OED)." *Habitat International* 37: 148–154. doi:10.1016/j.habitatint.2011.12.006.

Zhu, Q., S. Xu, and L. Han. 2007. "A New Shadow Extraction Method from Color Aerial Images Based on Dempster–Shafer Evidence theory." *ACTA Automatica Sinica* 33 (6): 588–595.